AGU PUBLICATIONS

Geophysical Research Letters

RESEARCH LETTER
10.1002/2015GL064811

Key Points:
- Bed-sediment cover strongly damps ground vibrations of debris flows
- Spectral power systematically increases as debris flow entrains bed sediment
- Bed-sediment thickness and entrainment rate can be inverted from geophone data

Supporting Information:
- Figures S1–S4
- Movie S1
- Movie S2

Correspondence to:
J. W. Kean,
jwkean@usgs.gov

Citation:
Kean, J. W., J. A. Coe, V. Coviello, J. B. Smith, S. W. McCoy, and M. Arattano (2015), Estimating rates of debris flow entrainment from ground vibrations, *Geophys. Res. Lett.*, *42*, 6365–6372, doi:10.1002/2015GL064811.

Received 3 JUN 2015
Accepted 17 JUL 2015
Accepted article online 22 JUL 2015
Published online 7 AUG 2015

Estimating rates of debris flow entrainment from ground vibrations

J. W. Kean[1], J. A. Coe[1], V. Coviello[2], J. B. Smith[1], S. W. McCoy[3,4], and M. Arattano[2]

[1]U.S. Geological Survey, Denver, Colorado, USA, [2]Italian National Research Council (CNR), Research Institute for Geo-hydrological Protection, Torino, Italy, [3]University of Nevada, Reno, Reno, Nevada, USA, [4]Geological Sciences and Engineering, Reno, Nevada, USA

Abstract Debris flows generate seismic waves as they travel downslope and can become more dangerous as they entrain sediment along their path. We present field observations that show a systematic relation between the magnitude of seismic waves and the amount of erodible sediment beneath the flow. Specifically, we observe that a debris flow traveling along a channel filled initially with sediment 0.34 m thick generates about 2 orders of magnitude less spectral power than a similar-sized flow over the same channel without sediment fill. We adapt a model from fluvial seismology to explain this observation and then invert it to estimate the level of bed sediment (and rate of entrainment) beneath a passing series of surges. Our estimates compare favorably with previous direct measurements of entrainment rates at the site, suggesting the approach may be a new indirect way to obtain rare field constraints needed to test models of debris flow entrainment.

1. Introduction

Debris flows can substantially increase their volume and destructive potential by entraining sediment as they travel downstream. Considerable progress has been made recently in the theory and modeling of sediment entrainment by debris flows [*Iverson and Ouyang*, 2015, and references therein]. Despite this progress, data sets needed to test models of entrainment are exceedingly rare due to the capricious and destructive nature of debris flows. Direct measurements of the entrainment rates of full-scale debris flows have only been obtained in a large-scale flume [*Iverson et al.*, 2011] and at two field sites [*Berger et al.*, 2011; *McCoy et al.*, 2012]. Entrainment by dry granular flows has also been studied in more manageable small-scale flumes [e.g., *Mangeney et al.*, 2010; *Farin et al.*, 2014]; however, these experiments lack the effects of pore-fluid pressure, which can substantially increase rates of entrainment [*Iverson et al.*, 2011; *McCoy et al.*, 2012]. Additional constraints on the total volume (but not rate) of eroded material are available from event-based topographic differencing [e.g., *Schürch et al.*, 2011; *Anderson et al.*, 2015]; however, the full depth of erosion can sometimes be obscured by deposition during the tail of the flow [e.g., *Staley et al.*, 2011].

Here in an effort to increase observations of sediment entrainment by debris flows, we explore an indirect method of measuring rates of debris flow erosion (and deposition) using ground vibrations recorded by geophones. Geophones have long been important tools in debris flow monitoring, but their application has been primarily focused on warning through event detection rather than on making quantitative measurements of debris flow processes [e.g., *Arattano*, 1999; *Hürlimann et al.*, 2003; *LaHusen*, 2005]. Recent work on large landslides has shown that aspects of flow dynamics, such as impact and shear forces, can be extracted from the seismograms of broadband networks [e.g., *Moretti et al.*, 2012; *Allstadt*, 2013]. Similarly, work in fluvial seismology has shown that important characteristics of river flow processes, such as bed load transport [e.g., *Govi et al.*, 1993; *Burtin et al.*, 2008; *Hsu et al.*, 2011; *Barrière et al.*, 2015] and turbulence [e.g., *Schmandt et al.*, 2013; *Gimbert et. al.*, 2014] are encoded in ground vibrations.

In this paper, we adapt a model from fluvial seismology [*Tsai et al.*, 2012] to address sediment entrainment by debris flows. Our analysis begins with new observations of debris flows at the Chalk Cliffs monitoring site in central Colorado. Measurements of ground vibrations, flow stage, and video show that debris flow-induced ground motion at the site is strongly damped by the presence of a thin ($\leq$0.34 m) layer of sediment covering the bedrock channel. These observations lead us to the hypothesis that the amplitude of ground vibrations is systematically related to the level of bed sediment in the channel, and that this relationship can be exploited to infer rates of debris flow erosion and deposition. To explore this hypothesis, we develop a simplified model for the ground vibrations generated by debris flows over an erodible bed. The model is inverted to estimate

the level of bed sediment (and rate of erosion) associated with a series of debris flow surges. Results compare favorably to previous direct measurements of debris flow entrainment using erosion sensors at the same site under similar conditions [*McCoy et al.*, 2012].

2. Study Site and Instrumentation

The Chalk Cliffs study site is located in a band of hydrothermally altered quartz monzonite in the Sawatch Range of central Colorado [*Coe et al.*, 2008]. The site experiences 3–4 debris flows per year between May and October. Debris flows are triggered by runoff from bedrock cliffs and sparsely vegetated hillslopes during rainstorms. The runoff rapidly (~5 min) mobilizes sediment accumulated in the channel from rock fall and dry ravel into debris flow [*Kean et al.*, 2013]. Of particular interest to this study are (1) recent direct measurements of debris flow entrainment rates using in situ erosion sensors [*McCoy et al.*, 2012], and (2) measurements of the distribution of bed-normal impact force at the base of debris flows [*McCoy et al.*, 2013]. We use the results from these two previous studies to develop and test the model presented in section 4.

Our field observations focus on the instrumented cross section at the upper station (Figure 1). Instrumentation includes a rain gage to measure rainfall intensity, a laser distance meter to measure flow stage (sampled at 10 Hz), a 232 cm^2 force plate to measure basal normal force (333 Hz), a 4.5 Hz triaxial geophone to measure ground vibrations (333 Hz), and a high-definition video camera to measure flow speed (23 frames per second) through particle tracking. The geophone is mounted to bedrock next to the channel, 3 m cross stream from the channel center line in which the force plate is mounted. The laser distance meter is suspended 2.94 m above the force plate. Bed-normal distance to the flow surface (or stationary bed surface) is converted to stage (H) above the force plate.

3. Observations

To illustrate the strong dependence of ground vibrations on bed-sediment thickness, we present observations of two different debris flow surges in Figure 2 (see also Movies S1 and S2 in the supporting information). The examples have comparable peak flow thicknesses (~0.6 m) but differ in the thickness of bed sediment (h_s) beneath the flow. The first example (4 July 2014) was triggered by the first significant rainstorm of the season and flowed over an initially dry sediment-covered bed ($h_s = 0.34$ m). This example generated much smaller amplitude ground vibrations than the second example (1 August 2014), which occurred later in the season and flowed over a bare bedrock channel ($h_s = 0$ m). In both cases, the largest vertical ground velocities (V) are associated with the peak stage at $t = 10$ s. The amplitudes of the horizontal ground velocities in both cases are also similar in magnitude to the vertical velocity (see Figure S1 in supporting information). This similarity suggests that both Rayleigh and Love surface waves may be present [*Gimbert et al.*, 2014]. Additional peaks in V are associated with rock falls (case 1, $t < 10$ s, Movie S1) and secondary, sediment-rich surges embedded in the tails (case 1, $t \sim 20$ s; case 2, $t \sim 38$ s, Movie S2).

Comparison of the power spectra (P^T) over 3 s following the peak stage (when flow conditions are not changing substantially) shows that the distribution of power in both cases is uniform with frequency; however, the mean power of case 1 ($h_s = 0.34$ m) is approximately 2 orders of magnitude less than case 2 ($h_s = 0$ m). The distribution in power is also observed to be uniform in moving windows across the time series (see spectrograms in Figure S1). A similar reduction in power with sediment thickness is observed at an auxiliary geophone 18 m downstream (see Figure S2). However, unlike the main geophone, this geophone, which is mounted in colluvium (2.9 m from the channel center), exhibits a more complicated frequency response, with more concentrated spectral power between 25 and 100 Hz after surge peaks (Figure S2). We suspect the difference in frequency response between the two geophones is the result of differences in the seismic characteristics of the mounting material, but additional frequency analysis is needed.

The observations in Figure 2 lead us to the hypothesis that the recorded ground velocities are surface waves generated primarily by the impacts of grains on bedrock sections of the channel. Grain impacts on more deformable loose bed sediment stored in the channel (if present) are suspected to generate negligibly small surface waves compared to impacts on bedrock, because impacts on sediment typically involve

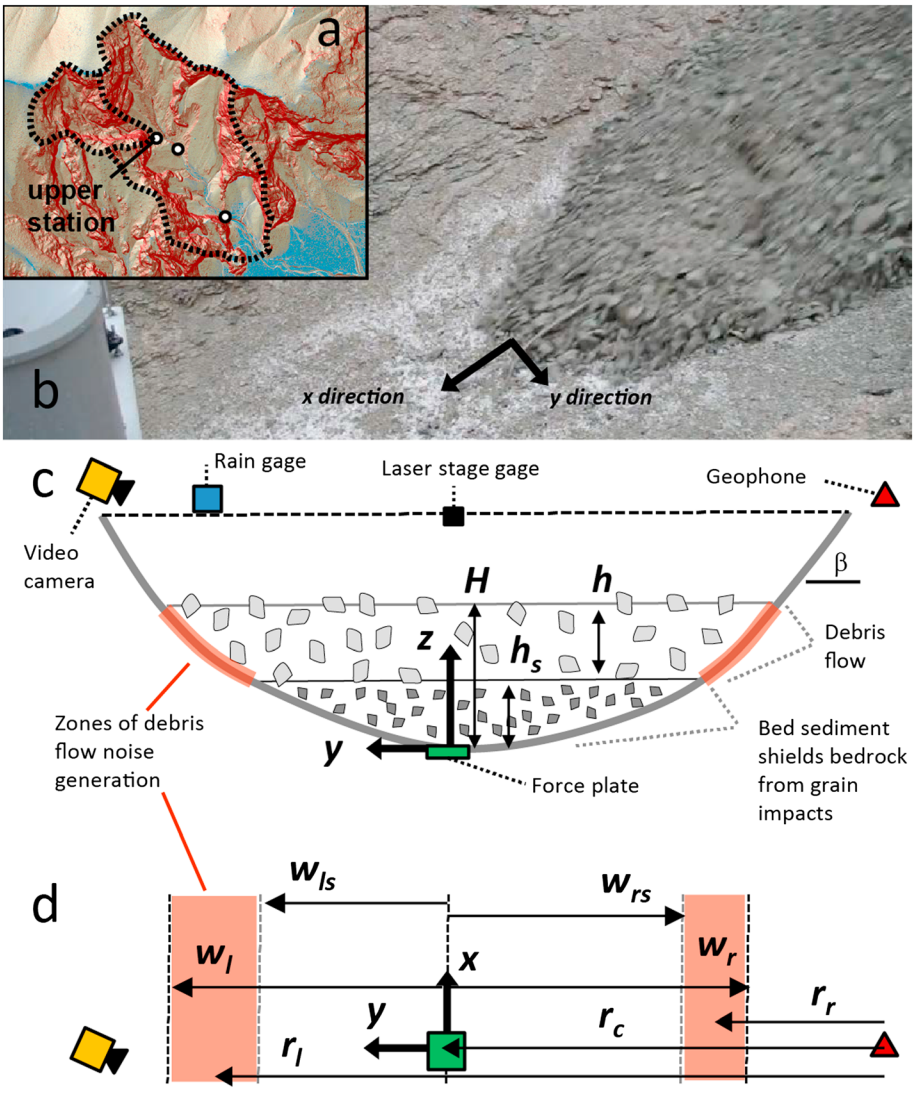

Figure 1. (a) Location of the upper station draining a 0.06 km^2 subbasin of Chalk Cliffs study area (396826N/4287850E, UTM zone 13). Red, grey, and blue shading indicates slopes above 45°, between 15° and 45°, and less than 15°, respectively. (b) Image of debris flow approaching the upper station on 4 July 2014. The view shows a 5.5 m length of channel upstream of the instrumented cross section. Diagram of (c) cross-stream view (looking downstream) and (d) planform view of reach and sensor locations. Shaded orange areas in Figures 1c and 1d indicate zones of seismic noise generation by grain impacts of debris flow. These zones grow in area as sediment is entrained from the bed. Grain impacts on bed sediment have been observed to generate negligible ground vibrations relative to impacts on bedrock.

inelastic collisions at multiple contact points that dissipate impact energy into friction. Thus, we expect *V* to increase as a function of the amount of bedrock exposed in the channel.

Ball drop tests at the site support our hypothesis that impacts on loose bed sediment result in negligible ground vibrations (see Figure S3). In these tests, a 1.8 kg metal sphere was dropped ~4 m away from the geophone from a height of ~1.5 m. One set of drops was on bedrock, and the other set on loose bed sediment ($h_s = 0.2$ m). Tests show that the maximum amplitude of *V* recorded from impacts on loose bed sediment was nearly an order of magnitude smaller than that recorded from impacts on rock and barely above the background noise level. Additional evidence for strong damping of bed sediment comes from force plate measurements at the site by *McCoy et al.* [2013]. Their measurements show that deviations from the measured mean basal force associated with particle impacts (typically 2–50 times larger than the mean) are almost completely damped by the presence of a thin 5 cm layer of bed sediment, regardless of whether the sediment was dry or saturated.

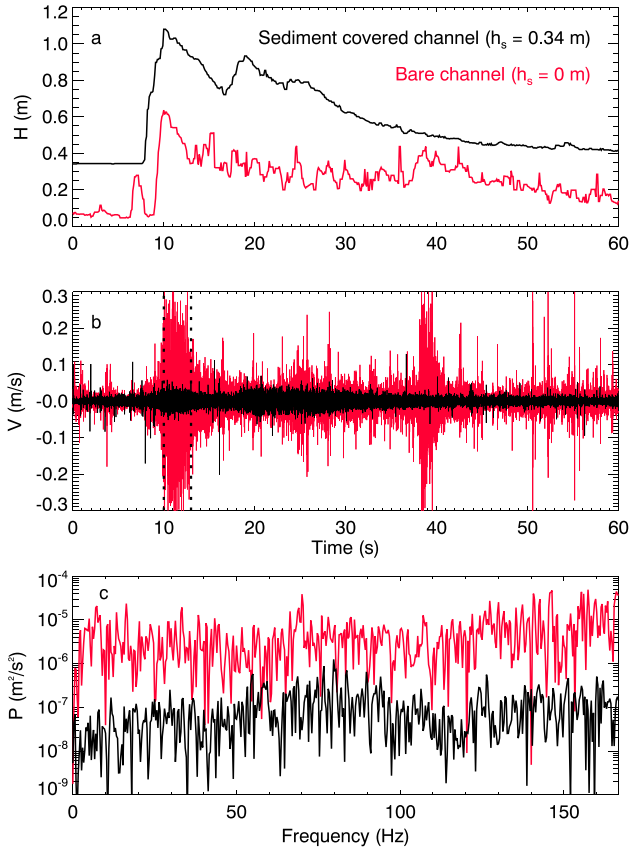

Figure 2. Comparison of (a) flow stage *H*, (b) vertical ground velocity *V*, and (c) power spectra *P* of debris flow surges recorded when the bedrock channel is bare (red) or covered with a 0.34 m layer of bed sediment (black). The power spectra correspond to a 3 s time window after the peak of both surges, which is shown with the dotted vertical lines in Figure 2b. Bed sediment cover is shown to have a substantial damping effect on debris flow induced ground vibrations at the site. See also Movies S1 and S2.

We focus here on the case of bed sediment confined to a streamwise uniform band in the center of a channel (Figure 1). In this case, the width of bed sediment cover (and bedrock exposure) is a systematic function of channel geometry and bed sediment thickness, h_s. We leave the more complicated situation of streamwise variability in sediment cover (i.e., random patches of bed sediment) for future study.

4. Model

To model the ground motions produced by debris flow impacts on bedrock, we follow an approach similar to the model of *Tsai et al.* [2012] for seismic noise generated by river bed load. In their model, the vertical ground velocity at a station is described by the sum of surface waves created from the impacts of individual grains saltating along the length of the river. Rayleigh waves from vertically incident impacts are assumed to be the primary waves causing motion in the vertical direction [*Sánchez-Sesma et al.*, 2011]. Using Hertzian contact mechanics [e.g., *Johnson*, 1987], *Tsai et al.* [2012] model the impulse to the bed from a grain impact as $I \approx (2/\pi)F_o\Delta t$, where F_o is the maximum force amplitude and Δt is the time of contact. They assume the impact is instantaneous relative to the frequency range of interest, such that the force history for a single impact can be described as $F_1(t) = I\delta(t)$, where $\delta(t)$ is the Dirac delta function. In our adaptation of the model of *Tsai et al.* [2012] to debris flows, we substitute river bed load impact forces with debris flow impact forces, which are constrained at our site by the basal force measurements of *McCoy et al.* [2013]. For simplicity, shear forces, which are estimated to only impart 18% of their energy into Rayleigh waves [*Sánchez-Sesma et al.*, 2011], are not included directly in the model; however, we expect the distribution of shear forces to scale with bed-normal forces following a Mohr-Coulomb relation.

For a given force time series $F(t)$ at streamwise position x_o and cross-stream position y_o, the vertical ground velocity $\dot{u}(t)$ at a station (position x, y) is given in the frequency domain by

$$\dot{u}(f,x,y) = 2\pi \, if \, F(f,x_o,y_o)G(f,r) \tag{1}$$

where f is frequency, $F(f, x_o, y_o)$ is the Fourier transform of $F(t)$, $G(f,r)$ is the displacement Green's function, and r is the station-source distance. For simplicity, we calculate this distance in two dimensions as $r = \sqrt{(x-x_o)^2 + (y-y_o)^2}$. *Tsai et al.* [2012] used a far-field approximation for the amplitude of the Rayleigh-wave Green's function. In condensed form, it is given by

$$|G(f,r)| \approx R(f) \sqrt{\frac{2}{\pi kr}} e^{-\alpha r} \tag{2}$$

where $\sqrt{2/(\pi kr)}$ represents the decay in wave amplitude from geometric spreading, $e^{-\alpha r}$ represents the decay in wave amplitude from energy loss, where α is the frequency-dependent attenuation coefficient for

bedrock, and $R(f) = k/(8\rho_s v_c v_u)$, where $k = 2\pi f/v_c$ is the angular wavenumber, ρ_s is the bedrock density, and v_c and v_u are the wave phase and group velocity, respectively.

We specify α in three whole-octave frequency bands (centered at 25, 50, and 100 Hz) by analyzing the growth in the amplitude of ground vibrations associated with an advancing surge toward the station (see Figure S4 in supporting information). Results from these calculations yield similar values for α in each band (0.18, 0.11, and 0.09 m^{-1}, respectively) and are slightly lower than values obtained for the colluvial channels (0.2–0.4 m^{-1}) studied by *Huang et al*. [2007]. To be consistent with the auxiliary geophone, which had peak power at intermediate frequencies, we focus on the middle band centered at 50 Hz.

Following *Tsai et al*. [2012], we assume impacts occur randomly in time such that the sum of impacts does not affect the shape of the force spectrum and $F(f) = F_1(f)\sqrt{N} = I\sqrt{N}$, where N is the total number of impacts. For a bare bedrock channel, the power spectral density (PSD) of a station's velocity time series (per unit impact force, F_o) can then be expressed as

$$P(f, F_o) = \int_{-w_r}^{w_l}\int_{-\infty}^{\infty} r_i |\dot{u}_1(f)|^2 \mathrm{d}x_o\, \mathrm{d}y_o \tag{3}$$

where w_l and w_r are the left and right margins of the flow, r_i is the rate of impact forces per unit area of the channel dA, and $\dot{u}_1(t)$ is the ground velocity due to $F_1(t)$. For rivers, *Tsai et al*. [2012] assume r_i is proportional to the rate of bed load transport. For debris flows, we assume r_i scales with the local surface flow velocity $u(x_o, y_o)$ such that $r_i \approx u(x_o, y_o)/(l_p \mathrm{d}A)$, where l_p is the length of the force plate where impacts are sampled. Video particle tracking shows that grains on the lateral margins of the debris flow move downstream at about half the velocity as grains in the center of the channel; and video of surge fronts indicates that the cross-stream variation in surface velocity is parabolic in shape (Figure 1b and Movies S1 and S2). Based on these observations, we model $u(x_o, y_o)$ to vary across the channel as $u(x_o, y_o) = u_c[1 - 0.5(y/w)^2]$, where u_c is the surface velocity in the center of the channel and w is the lateral distance to the margin of the flow. We assume u_c can vary from surge to surge and along the length of an individual surge and determine its value from video footage.

To address the case of flow over a sediment-filled channel, the cross-stream limits of integration in equation (3) are modified to include only inundated bedrock portions of the channel (in keeping with our observation that impacts on sediment-covered sections of the channel are damped). This case splits the cross-stream integral into a left and right half whose inner limits of integration (w_{ls} and w_{rs}) are functions of h_s and channel cross-section geometry (Figure 1). The left and right halves of the integral grow in width as erosion progresses and more bedrock is exposed.

The total PSD at a station from bed impacts is found by integrating equation (3) over the distribution of impact forces in the debris flow

$$P^T(f) = \int_{F_o} P(f, F_o)\mathrm{d}F_o \tag{4}$$

Using observations from five debris flows, *McCoy et al*. [2013] showed that bed normal impact forces in both sediment-rich surge peaks and more watery tails follow a generalized Pareto distribution that scales with the mean time-averaged basal normal force, $\overline{F}(t)$. These observations simplify the force part of our problem to a description of the mean basal normal forces beneath the flow. Additional work is needed to see if this scaling holds for other flow situations. For flow parallel to the longitudinal bed slope, $\overline{F}(t)$ scales with the local flow thickness (h) and flow density (ρ) through the relation $\overline{F}(t) = \rho g(\cos\theta)(\cos\beta)h\mathrm{d}A$, where g is the acceleration of gravity and θ and β are the bed slope angles in the downstream and cross-stream directions, respectively.

The seismic wave parameters in the term $R(f)$ of equation (2) are not known at our site. Rather than estimate their values from the literature following *Tsai et al*. [2012], we eliminate the unknown term by analyzing the spectral ratio of $P^T(f)$ to a reference observation $P_b^T(f)$ made at the same station [e.g., *Båth*, 1974]. Our reference power spectrum corresponds to the one shown in Figure 2c for the peak of the bare channel surge ($u_c = 6.3$ m/s).

To simplify equations (3) and (4), and minimize the effects of unresolved variations in flow density and surge shape, we restrict our analysis to times when surge peaks (which have the largest impacts and most consistent flow density) are closest to the station. This restriction allows us to approximate $P^T(f)/P_b^T(f)$ for

bare channel flows as the ratio of the power spectra generated by two point sources located in the center of the channel at the station cross section. The point-source approximation reduces the spectral ratio to a function of bulk flow properties given by

$$\frac{P^T(f)}{P_b{}^T(f)} \approx \frac{\left[\rho H W u_c (e^{-\alpha r_c})/\sqrt{r_c}\right]^2}{\left[\rho_b H_b W_b u_{c\,b} (e^{-\alpha r_c})/\sqrt{r_c}\right]^2} \tag{5}$$

where H is the measured flow stage (corresponding to flow thickness h for the bare channel case), W is the width of the flow, r_c is the distance from the station to the channel center, and the subscript b denotes flow properties of the reference bare channel case. Equation (5) can be further simplified by canceling $(e^{-\alpha r_c})/\sqrt{r_c}$ and assuming $\rho \approx \rho_b$. Video observations of surge texture suggest this is a reasonable approximation for surge peaks. The accuracy of equation (5) compared to the integration of grain impacts along the length and width of a surge is described in Figure S5. We find that for $0.9 < H/H_b < 1.1$, equation (5) is within 10% of the complete solution and within 30% for $0.65 < H/H_b < 1.3$. Full integration of equations (3) and (4) should be used in situations where there is a larger difference between H and H_b.

To address the case of a sediment-filled channel, the numerator in equation (5) is modified to represent two point sources located in the centers of the left ($r = r_l$) and right ($r = r_r$) exposed bedrock sections of the channel

$$\frac{P^T(f)}{P_b^T(f)} = \frac{\left[\rho h(r_r) W_r u(r_r) \cos(\beta_r)(e^{-\alpha r_r})/\sqrt{r_r}\right]^2 + \left[\rho h(r_l) W_l u(r_l) \cos(\beta_l)(e^{-\alpha r_l})/\sqrt{r_l}\right]^2}{\left[\rho_b H_b W_b u_{cb} (e^{-\alpha r_c})/\sqrt{r_c}\right]^2} \tag{6}$$

where $W_r = |w_r - w_{rs}|$, $W_l = |w_l - w_{ls}|$, and β_l and β_r are the cross-stream slope angles at $r = r_l$ and r_r, respectively. The local flow thicknesses $h(r_l)$ and $h(r_r)$ at the centers of the exposed left and right sides of the channel are functions of H and h_s. For a given observation of ground motion during a surge peak, we use a root-finding method to solve equation (6) for h_s. We specify $P^T(f)$ and $P_b^T(f)$ in the band centered at 50 Hz using a 3 s time window following the surge peak.

5. Results

We apply the model to estimate h_s and rate of erosion during the 4 July 2014 debris flow introduced in Figure 2. The full event consists of seven quasi-periodic surges that eventually erode most of the dry bed material (Figure 3 and Movie S1). Each surge has a different u_c at peak flow, which is labeled in the figure. As the surges pass the station there is a gradual increase in ground velocity V, indicating erosion is taking place along the reach. The growth in amplitude is particularly noticeable in the 1 s averaged envelope of V, which roughly matches the shape of each surge. For the first four surges, the model predicts progressive erosion at an average rate of 2 mm/s. Deposition is predicted beneath the fifth and last surge. Comparison of the stage and force time series, which has been scaled to superimpose when $\rho = 2100\ \mathrm{kg/m^3}$, suggests the assumption of constant ρ at surge peaks is reasonable for this event, but it may not be valid universally.

Model results can be evaluated using previous direct measurements of erosion at the same location under similar bed and flow conditions (dry bed sediment with $0.36 < h_s < 1.1$ and multiple surges with $0.51 < H < 1.1$ and $3.0 < u_c < 4.6$) [*McCoy et al.*, 2012]. Additional qualitative tests on the model come from independent constraints on h_s from the stage gage, video, and force plate, which, for example, did not record large impact forces directly on the plate, indicating it was never fully exposed to the flow. The modeled entrainment rate during the first four surges is within the range of the *McCoy et al.* [2012] direct measurements for four debris flow events over dry bed sediment (2, 3, 3, and 5 mm/s).

Results from the last three surges reveal limitations of the model for estimating reach-scale entrainment. As seen in the video, these later surges expose the uneven bedrock topography underlying the initially smooth sediment-covered bed. For example, prior to the arrival of the last surge ($t \sim 320$ s), video shows that much of the reach upstream of the cross section is sediment free, while the force plate indicates that at least 5 cm of bed sediment remains in the central part of the cross section (based on the absence of large force excursions). The layer of sediment covering the force plate, which is just out of range of the camera view, is likely associated with deposition that often occurs downstream of the cross section due to a decrease in channel slope from ~15° upstream to ~10° downstream (see Figure S6). Downstream deposition of the small fourth and sixth surges may also be responsible for the predicted increase in h_s beneath surge five

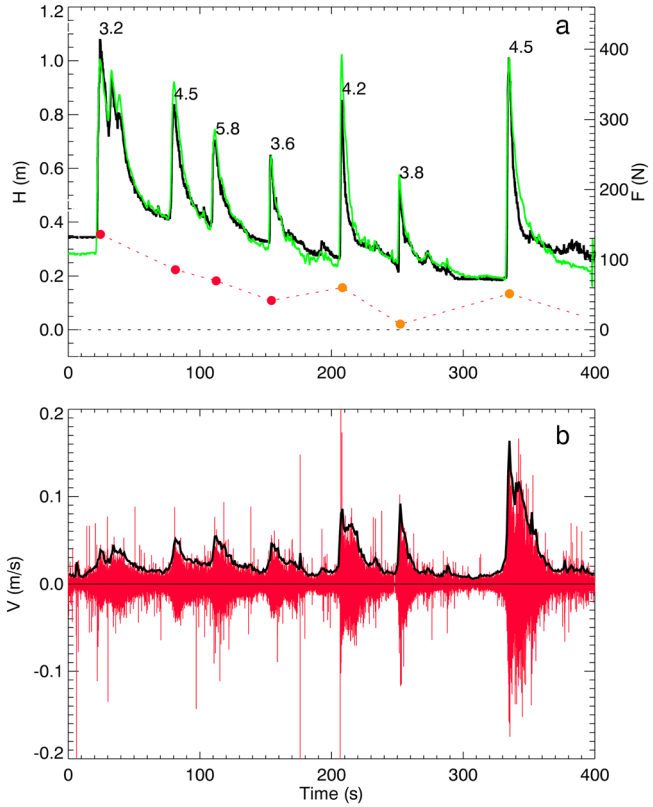

Figure 3. (a) Measured debris flow stage (black), modeled bed sediment thickness h_s, (dots), and measured 1 s averaged basal normal force (green) during the 4 July 2014 event. The force axis is scaled such that H and $F = \rho g H \cos(\theta) I_p^2$, superimpose with $\rho = 2100$ kg/m^3. This scaling highlights time variability in ρ. When F plots below H, ρ is less than 2100 kg/m^3, and when F plots above H, ρ is greater than 2100 kg/m^3. Measured velocities at the peak of each surge are listed in meter per second. (b) Associated ground vibrations at the geophone (red) and 1 s averaged envelope with four times vertical exaggeration (black). Model estimates for average h_s during the last three surges ($t > 200$ s, orange dots) are considered less reliable due to variable bed conditions not resolved in the model.

and seven. Although these estimates of local deposition are consistent with the force plate, independent measures of h_s at the cross section are not available to evaluate their accuracy. The complication of a longitudinally uneven sediment distribution, which develops after substantial erosion has taken place, is not addressed by our simple model. In addition, flow effects associated with the irregular channel topography alter $\overline{F}(t)$ from the lithostatic assumption of the model. Given these two complications, model predictions of average h_s can only be considered reliable for the first four surges, when the assumptions of the model are consistent with the flow conditions.

6. Discussion and Conclusions

Presently, our model is limited to bedrock channels filled with sediment. Although bedrock channels are common in steep lands susceptible to debris flow, it is not clear if the approach could be adapted to detect debris flow entrainment in colluvial channels. Presumably, a colluvial channel would have a less distinct relation between P^T and h_s than observed in our sediment-filled bedrock channel, due to a weaker contrast in seismic characteristics between the eroding and stationary channel material. In the case of uniform channel material (colluvium or bedrock), geophones could alternatively be used to distinguish changes in flow density ρ relative to a reference condition using the approximation in equation (5) or full integration of equations (3) and (4). Additional study is needed to evaluate the accuracy of such density estimates.

Although further testing is needed, our initial results show a promising new use for an old tool in debris flow monitoring. Indirect measurements of debris flow entrainment rates using complementary observations of ground motion, signal attenuation, flow stage, and velocity could provide rare field constraints needed to test theories and models of debris flow entrainment. In addition, the predicted increase in h_s after the fourth surge ($t \sim 200$ s) suggests that the approach may also be used to estimate rates of deposition during a debris flow, a field measurement that is extremely difficult to make by other means. Additional work is needed to understand the effects of flow density, grain size, and longitudinal variations in bed sediment coverage on observed ground motions.

Our observation that thin layers of bed sediment strongly damp debris flow induced ground motions has implications for other problems besides entrainment. Most importantly, use of geophones to provide debris flow warning requires a threshold level of ground vibration to trigger alarms [e.g., *Badoux et al.*, 2008; *Abancó et al.*, 2014]. Changes in the levels of bed sediment at a site, such as those from accumulation of dry ravel or rockfall, could substantially alter the threshold for detection. Our results for debris flows may also be relevant to monitoring sediment transport in bedrock rivers. Given the strong

sediment damping effects at Chalk Cliffs, it is reasonable to expect that impacts from saltating grains on sediment-covered portions of a river bed could generate substantially different amplitude ground vibrations than impacts on exposed bedrock. Neglecting this difference could potentially lead to errors in interpreting bed load transport rates from seismic data.

Acknowledgments
We thank Victor Tsai, Kate Allstadt, and an anonymous reviewer for their thoughtful reviews of the manuscript. Data for the complete events shown in Figures 2 and 3 are available at ftp://ftpext.usgs.gov/pub/cr/co/golden/Kean/DebrisFlowErosion. Partial support for V. Coviello came from a CNR short-term mobility project.

The Editor thanks Victor Tsai and an anonymous reviewer for their assistance in evaluating this paper.

References

Abancó, C., M. Hürlimann, and J. Moya (2014), Analysis of the ground vibration generated by debris flows and other torrential processes at the Rebaixader monitoring site (Central Pyrenees, Spain), *Nat. Hazards Earth Syst. Sci.*, *14*(4), 929–943, doi:10.5194/nhess-14-929-2014.

Allstadt, K. (2013), Extracting source characteristics and dynamics of the August 2010 Mount Meager landslide from broadband seismograms, *J. Geophys. Res. Earth Surf.*, *118*, 1472–1490, doi:10.1002/jgrf.20110.

Anderson, S. W., S. P. Anderson, and R. S. Anderson (2015), Exhumation by debris flows in the 2013 Colorado Front Range storm, *Geology*, *43*, 391–394, doi:10.1130/G36507.1.

Arattano, M. (1999), On the use of seismic detectors as monitoring and warning systems for debris flows, *Nat. Hazards*, *20*, 197–213.

Badoux, A., C. Graf, J. Rhyner, R. Kuntner, and B. W. McArdell (2008), A debris-flow alarm system for the Alpine Illgraben catchment: Design and performance, *Nat. Hazards*, *49*(3), 517–539, doi:10.1007/s11069-008-9303-x.

Barrière, J., A. Oth, R. Hostache, and A. Krein (2015), Bed load transport monitoring using seismic observations in a low-gradient rural gravel bed stream, *Geophys. Res. Lett.*, *42*, 2294–2301, doi:10.1002/2015GL063630.

Båth, M. (1974), *Spectral Analysis in Geophysics*, 563 pp., Elsevier, Amsterdam.

Berger, C., B. McArdell, and F. Schlunegger (2011), Direct measurement of channel erosion by debris flows, Illgraben, Switzerland, *J. Geophys. Res.*, *116*, F01002, doi:10.1029/2010JF001722.

Burtin, A., L. Bollinger, J. Vergne, R. Cattin, and J. L. Nábělek (2008), Spectral analysis of seismic noise induced by rivers: A new tool to monitor spatiotemporal changes in stream hydrodynamics, *J. Geophys. Res.*, *113*, B05301, doi:10.1029/2007JB005034.

Coe, J. A., D. A. Kinner, and J. W. Godt (2008), Initiation conditions for debris flows generated by runoff at Chalk Cliffs, central Colorado, *Geomorphology*, *96*(3–4), 270–297, doi:10.1016/j.geomorph.2007.03.017.

Farin, M., A. Mangeney, and O. Roche (2014), Fundamental changes of granular flow dynamics, deposition, and erosion processes at high slope angles: Insights from laboratory experiments, *J. Geophys. Res. Earth Surf.*, *119*, 504–532, doi:10.1002/2013JF002750.

Gimbert, F., V. C. Tsai, and M. P. Lamb (2014), A physical model for seismic noise generation by turbulent flow in rivers, *J. Geophys. Res. Earth Surf.*, *119*, 2209–2238, doi:10.1002/2014JF003201.

Govi, M., F. Maraga, and F. Moia (1993), Seismic detectors for continuous bedload monitoring in a gravel stream, *Hydrol. Sci. J.*, *38*(2), 123–132, doi:10.1080/02626669309492650.

Hsu, L., N. J. Finnegan, and E. E. Brodsky (2011), A seismic signature of river bedload transport during storm events, *Geophys. Res. Lett.*, *38*, L13407, doi:10.1029/2011GL047759.

Huang, C.-J., H.-Y. Yin, C.-Y. Chen, C.-H. Yeh, and C.-L. Wang (2007), Ground vibrations produced by rock motions and debris flows, *J. Geophys. Res.*, *112*, F02014, doi:10.1029/2005JF000437.

Hürlimann, M., D. Rickenmann, and C. Graf (2003), Field and monitoring data of debris-flow events in the Swiss Alps, *Can. Geotech. J.*, *40*, 161–175.

Iverson, R. M., and C. Ouyang (2015), Entrainment of bed material by Earth-surface mass flows: Review and reformulation of depth-integrated theory, *Rev. Geophys.*, *53*, 27–58, doi:10.1002/2013RG000447.

Iverson, R. M., M. E. Reid, M. Logan, R. G. Lahusen, J. W. Godt, and J. P. Griswold (2011), Positive feedback and momentum growth during debris-flow entrainment of wet bed sediment, *Nat. Geosci.*, *4*, 116–121.

Johnson, K. L. (1987), *Contact Mechanics*, 452 pp., Cambridge Univ. Press, New York.

Kean, J. W., S. W. McCoy, G. E. Tucker, D. M. Staley, and J. A. Coe (2013), Runoff-generated debris flows: Observations and modeling of surge initiation, magnitude, and frequency, *J. Geophys. Res. Earth Surf.*, *118*, 2190–2207, doi:10.1002/jgrf.20148.

LaHusen, R. (2005), Debris-flow instrumentation, in *Debris-flow Hazards and Related Phenomena*, edited by M. Jakob and O. Hunger, pp. 291–304, Praxis, Heidelberg.

Mangeney, A., O. Roche, O. Hungr, N. Mangold, G. Faccanoni, and A. Lucas (2010), Erosion and mobility in granular collapse over sloping beds, *J. Geophys. Res.*, *115*, F03040, doi:10.1029/2009JF001462.

McCoy, S. W., J. W. Kean, J. A. Coe, G. E. Tucker, D. M. Staley, and T. A. Wasklewicz (2012), Sediment entrainment by debris flows: In situ measurements from the headwaters of a steep catchment, *J. Geophys. Res.*, *117*, F03016, doi:10.1029/2011JF002278.

McCoy, S. W., G. E. Tucker, J. W. Kean, and J. A. Coe (2013), Field measurement of basal forces generated by erosive debris flows, *J. Geophys. Res. Earth Surf.*, *118*, 589–602, doi:10.1002/jgrf.20041.

Moretti, L., A. Mangeney, Y. Capdeville, E. Stutzmann, C. Huggel, D. Schneider, and F. Bouchut (2012), Numerical modeling of the Mount Steller landslide flow history and of the generated long period seismic waves, *Geophys. Res. Lett.*, *39*, L16402, doi:10.5167/uzh-68355.

Sánchez-Sesma, F. J., R. L. Weaver, H. Kawase, S. Matsushima, F. Luzón, and M. Campillo (2011), Energy partitions among elastic waves for dynamic surface loads in a semi-infinite solid, *Bull. Seismol. Soc. Am.*, *101*(4), 1704–1709, doi:10.1785/0120100196.

Schmandt, B., R. C. Aster, D. Scherler, V. C. Tsai, and K. Karlstrom (2013), Multiple fluvial processes detected by riverside seismic and infrasound monitoring of a controlled flood in the Grand Canyon, *Geophys. Res. Lett.*, *40*, 4858–4863, doi:10.1002/grl.50953.

Schürch, P., A. L. Densmore, N. J. Rosser, and B. W. McArdell (2011), Dynamic controls on erosion and deposition on debris-flow fans, *Geology*, *39*(9), 827–830, doi:10.1130/G32103.1.

Staley, D. M., T. A. Wasklewicz, J. A. Coe, J. W. Kean, S. W. McCoy, and G. E. Tucker (2011), Observations of debris flows at Chalk Cliffs, Colorado, USA: Part 2, Changes in surface morphometry from terrestrial laser scanning in the summer of 2009, in *Debris-flow Hazards Mitigation, Mechanics, Prediction, and Assessment*, edited by R. Genevois, D. L. Hamilton, and A. Prestininzi, pp. 759–768, Casa Editrice Universita La Sapienza, Rome, doi:10.4408/IJEGE.2011-03.B-083.

Tsai, V. C., B. Minchew, M. P. Lamb, and J.-P. Ampuero (2012), A physical model for seismic noise generation from sediment transport in rivers, *Geophys. Res. Lett.*, *39*, L02404, doi:10.1029/2011GL050255.